Size quantization of excitons in microcrystals with large longitudinal-transverse splitting

A. I. Ekimov, A. A. Onushchenko, M. É. Raĭkh, and Al. L. Éfros

A. F. Ioffe Physicotechnical Institute, Academy of Sciences of the USSR, Leningrad

(Submitted 29 October 1985)
Zh. Eksp. Teor. Fiz. **90**, 1795–1807 (May 1986)

An investigation is made of the luminescence spectra of CuCl microcrystals grown in an insulating matrix of silicate glass. A doublet structure of a resonance exciton luminescence line is found in the microcrystal size range $a \sim 50$–150 Å when the separation between the size-quantization levels is of the order of the longitudinal-transverse splitting of the exciton spectrum. A theory of size quantization of an exciton in a semiconductor sphere is developed allowing for the longitudinal-transverse splitting. It is found that the observed anomalous structure of the luminescence spectrum is due to a strong increase in the rate of exciton transitions when the positions of exciton lines governed by size quantization coincide with the frequency of a surface electromagnetic wave mode.

1. INTRODUCTION

Studies of three-dimensional semiconductor microcrystals grown in transparent insulating matrices are being pursued vigorously. Such heterophase systems make it possible to study the effects of size quantization in semiconductors, because this microcrystal growth method makes it possible to vary their size in a controlled manner over a wide range from a few tens of thousands or more angstroms.[1] The transparency of the silicate glass matrix in a wide range of wavelengths from ultraviolet to the near infrared makes it possible to employ conventional optical spectroscopy methods in studies of such systems. Size quantization of the energy spectrum of free electrons is manifest in the interband absorption spectra of CdS microcrystals.[2] Size quantization of excitons has been observed and studied in the absorption and luminescence spectra of CuCl microcrystals.[3,4]

We report the structure of a resonance exciton luminescence line of CuCl microcrystals which appears when their size is $a \sim 50$–150 Å.

We show that the observed structure is associated with a large longitudinal-transverse splitting $\hbar\omega_{LT}$ of the exciton spectrum of CuCl crystals ($\hbar\omega_{LT} = 5.7$ meV is given in Ref. 5), and is due to a strong reduction in the radiative lifetime of excitons in microcrystals when the positions of exciton lines governed by the size quantization of the energy spectrum coincide with the frequency of a surface electromagnetic wave mode (surface exciton frequency).

In Sec. 2 we shall give the experimental results and carry out a qualitative analysis of the observed pattern. A theory of size quantization of excitons allowing for the longitudinal-transverse splitting is presented in Secs. 3 and 4. The results obtained are compared with the theory in Sec. 5.

2. EXPERIMENTAL RESULTS

Microcrystals of CuCl were grown by diffusive phase precipitation of a supersaturated solid solution in the interior of a silicate glass matrix by a method described in Ref. 1. The average microcrystal radius was determined for each sample by the small-angle x-ray scattering method. The luminescence spectra of microcrystals were recorded using an SDL-1 spectrometer on excitation with the $\lambda = 3642$ Å krypton laser line of 50 mW power. The spectra were recorded at $T = 4.2$ K.

Figure 1a shows the luminescence spectra of CuCl microcrystals as a function of their average radius $\bar{a}$. The spectral position and width of the $\lambda = 3902$ Å line governed by the annihilation of excitons bound to neutral acceptors were independent of the microcrystal size. The position of the resonance exciton luminescence line in the range of small sizes ($\bar{a} < 50$ Å) is governed, as was shown earlier, by size quanti-

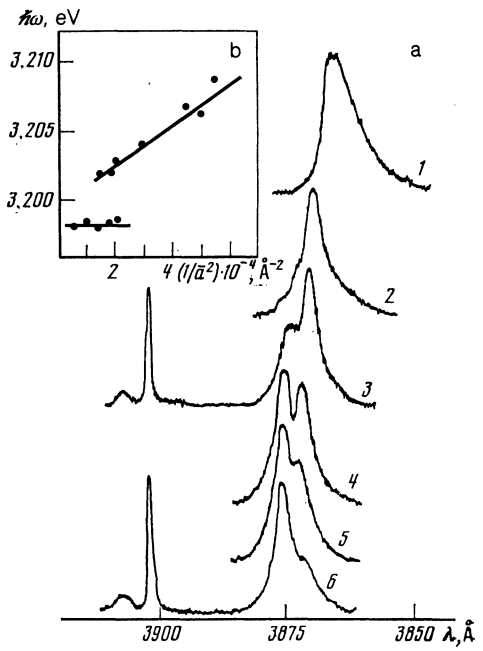

FIG. 1. a) Resonance exciton luminescence spectra obtained for different values of the average radius of CuCl microcrystals: 1) $\bar{a} = 45$ Å; 2) $\bar{a} = 56$ Å; 3) $\bar{a} = 70$ Å; 4) $\bar{a} = 76$ Å; 5) $\bar{a} = 95$ Å; 6) $\bar{a} = 132$ Å. b) Dependence of the positions of the maxima of the doublet structure on the average radius of microcrystals.

 0038-5646/86/051054-07$04.00 © 1986 American Institute of Physics

zation of excitons and was described satisfactorily (see Fig. 1b) by the following expression[4]

$$\hbar\omega=\hbar\omega_T+\hbar^2\pi^2/2ma^2, \tag{1}$$

where $\hbar\omega_T$ is the position of the bottom of the exciton subband and m is the translation mass of an exciton.

When the microcrystal size was increased, a second line appeared in the resonance exciton luminescence spectrum when the size reached $\bar{a}\sim 70$–80 Å, but the position of this line was independent of the microcrystal size (Fig. 1b). When the microcrystal size was increased further, this line dominated the spectrum. The appearance of a line with a position independent of the microcrystal size can be understood if we ignore spatial dispersion associated with the motion of an exciton as a whole, which corresponds to the limit $m\to\infty$.

In fact, if we ignore spatial dispersion associated with the motion of an exciton as a whole, the interaction of a semiconductor sphere with light can be described by the macroscopic permittivity $\varkappa(\omega)$ given by the following expression[6] in the range of frequencies ω close to the exciton line:

$$\varkappa(\omega)=\varkappa_\infty(1-\omega_{LT}/(\omega-\omega_T)), \tag{2}$$

where $\varkappa_\infty$ is the high-frequency permittivity and ω_T is the frequency corresponding to the bottom of the exciton subband; $\varkappa(\omega)$ is negative at frequencies ω defined by

$$\omega_T<\omega<\omega_L=\omega_T+\omega_{LT}.$$

The solution of the Maxwell equations gives, for this case, surface modes of frequencies ω_s^F which are found from the condition[7]:

$$\varkappa(\omega_s^F)+(F+1)\varkappa_m/F=0, \tag{3}$$

where $\varkappa_m$ is the permittivity of the matrix and F is the total angular momentum describing the spatial distribution of the electromagnetic field. It follows from Eqs. (2) and (3) that

$$\omega_s^F=\omega_T+\omega_{LT}\frac{\varkappa_\infty}{\varkappa_\infty+\varkappa_m(F+1)/F}. \tag{4}$$

Only the state with $F=1$ is optically active. We can see that the frequencies ω_s^F are independent of the radius of the sphere. This is due to neglect of the spatial dispersion.

Using Eqs. (1) and (4), we can readily estimate the shift of an exciton level due to size quantization, which is of the order of the longitudinal-transverse splitting in the case of microcrystals with $a\sim 70$–80 Å, i.e., precisely in the size range in which a doublet structure appears in the spectrum. Therefore, the structure of the exciton spectrum can be described in this range of sizes by developing a theory of size quantization of excitons which allows for the longitudinal-transverse splitting of the exciton spectrum.

3. ENERGY SPECTRUM AND RADIATIVE LIFETIME OF AN EXCITON IN A SPHERE

The system of equations relating the exciton component of the polarization $\mathbf{P}(\mathbf{r})$ to the electric field $\mathbf{E}(\mathbf{r})$ in a sphere is[8]

$$-\frac{\hbar^2}{2m}\Delta\mathbf{P}-\varepsilon\mathbf{P}=\alpha\mathbf{E}, \tag{5}$$

$$\text{curl curl}\,\mathbf{E}=\frac{\omega^2}{c^2}\mathbf{D}=\frac{\omega^2}{c^2}(\varkappa_\infty\mathbf{E}+4\pi\mathbf{P}), \tag{6}$$

where c is the velocity of light; $\mathbf{D}$ is the induction vector; $\varepsilon=\hbar(\omega-\omega_T)$; $\alpha=\varkappa_\infty\hbar\omega_{LT}/4\pi$. The interaction of an exciton with the electric field in such a sphere is governed by the value of the interband matrix element $\mathscr{P}$, which also occurs in the expression for the longitudinal-transverse splitting $\omega_{LT}\propto\mathscr{P}^2$. In the usual scheme for the calculation of the radiative lifetime of an exciton the right-hand side of Eq. (5) should be regarded as small, i.e., the interaction of an exciton with light can be allowed for using perturbation theory. In this approach the positions of size quantization levels are independent of $\mathscr{P}$ and, consequently, of ω_{LT}, and the lifetime is inversely proportional to $\mathscr{P}^2$. As pointed out in the Introduction, in this case the level position ε and the longitudinal-transverse splitting are quantities of the same order of magnitude, so that the interaction of an exciton with the electric field cannot be treated using perturbation theory. It is then found that the positions of the size quantization levels depend strongly, via ω_{LT}, on the matrix element and the lifetime depends on $\mathscr{P}$ in a more complicated manner.

Since in addition to the positions of the size quantization levels we are interested in the radiative lifetime, we find it convenient to solve the problem as follows. We consider the scattering of an electromagnetic wave by a semiconductor sphere. The solutions of the system (5)–(6) are characterized by the total angular momentum F because of the spherical symmetry of the problem. The partial scattering cross section σ_F is[9]

$$\sigma_F=2\pi c^2\omega^{-2}(2F+1)\sin^2\delta_F, \tag{7}$$

where δ_F is the scattering phase. If the wave frequency is close to one of the frequencies $\omega_F^{(n)}$ due to resonant creation of excitons at a size quantization level, the scattering phase δ_F can be represented by

$$\delta_F=\operatorname{arctg}\frac{\Gamma_F^{(n)}}{\omega-\omega_F^{(n)}}. \tag{8}$$

Then, the position of a size quantization level is given by $\varepsilon_F^n=\hbar(\omega_F^{(n)}-\omega_T)$, whereas the radiative time is given by $\tau_F^{(n)}=1/\Gamma_F^{(n)}$. Therefore, the problem reduces to finding the scattering phases. To do this, we must match solutions of the system (5)–(6) at the boundary of the investigated sphere where $r=a$ to the solutions of the Maxwell equations outside the sphere. Moreover, we shall assume that the exciton contribution to the polarization satisfies the Pekar condition $\mathbf{P}(a)=0$ (Ref. 6).

For a given value of the momentum F ($F=0,1,2,3,\ldots$) the solutions of the system (5)–(6) exhibit $(2F+1)$-fold degeneracy with respect to the projection of the momentum M. For fixed values of F and M, these solutions can be found by expanding in terms of the spherical vectors

$$\mathbf{P}_{F,M}(\mathbf{r})=u(r)\mathbf{Y}_{F,F,M}+u^+(r)\mathbf{Y}_{F,F+1,M}+u^-(r)\mathbf{Y}_{F,F-1,M}, \tag{9}$$

$$\mathbf{E}_{F,M}(\mathbf{r})=v(r)\mathbf{Y}_{F,F,M}+v^+(r)\mathbf{Y}_{F,F+1,M}+v^-(r)\mathbf{Y}_{F,F-1,M}, \tag{10}$$

where the spherical vectors $\mathbf{Y}_{F,l_F,M}(\Omega)$ represent three-component columns and are eigenfunctions of the total momentum operator

$$\hat{\mathbf{F}}\mathbf{Y}_{F,\,l_F,\,M}=F\mathbf{Y}_{F,\,l_F,\,M}, \tag{11}$$

where $\hat{\mathbf{F}}=\hat{\mathbf{l}}+\hat{\mathbf{I}}$; $\hat{\mathbf{l}}$ is the orbital momentum operator; and $\hat{\mathbf{I}}$ is the linear momentum operator with the value 1. Its projections I_x, I_y, and I_z are 3×3 matrices. The projections of the vectors $\mathbf{P}$ and $\mathbf{E}$ in Eqs. (9) and (10) are governed by the appropriate rows of the columns that occur on the right-hand side. The explicit form of the operator $\hat{\mathbf{I}}$ and of the functions $\mathbf{Y}_{F,l_F,M}(\Omega)$ is given in Ref. 10. The functions $\mathbf{Y}_{F,F-1,M}(\Omega)$ and $\mathbf{Y}_{F,F+1,M}(\Omega)$ have the same parity, which differs from the parity of the function $\mathbf{Y}_{F,F,M}$, so that the system of equations describing the radial functions u, u^+, u^- and v, v^+, v^- separates into two independent systems. The first relates the functions u and v and the second the functions u^+, u^-, v^+, and v^-. We shall give only the second system of equations because—as demonstrated later—only the solutions of this equation are important in the interpretation of the experiments. This second system is

$$\begin{aligned}
&-\frac{\hbar^2}{2m}\Delta_{F-1}u^- -\varepsilon u^- =\alpha v^-, \quad -\frac{\hbar^2}{2m}\Delta_{F+1}u^+ -\varepsilon u^+ =\alpha v^+,\\
&\frac{F+1}{2F+1}\Delta_{F-1}v^- +\frac{[F(F+1)]^{1/2}}{2F+1}\hat{T}^-_{F+1}v^+ =-\frac{\omega^2}{c^2}(\varkappa_\infty v^- +4\pi u^-),\\
&\frac{F}{2F+1}\Delta_{F+1}v^+ +\frac{[F(F+1)]^{1/2}}{2F+1}\hat{T}^+_{F-1}v^- =-\frac{\omega^2}{c^2}(\varkappa_\infty v^+ +4\pi u^+),
\end{aligned} \tag{12}$$

where the operators Δ_l, $\hat{T}_l{}^+$, and $\hat{T}_l{}^-$ are defined as follows:

$$\Delta_l=\frac{1}{r^2}\frac{\partial}{\partial r}\left(r^2\frac{\partial}{\partial r}\right)-\frac{l(l+1)}{r^2}, \tag{13}$$

$$\hat{T}_l{}^+=\left(-\frac{\partial}{\partial r}+\frac{l+1}{r}\right)\left(-\frac{\partial}{\partial r}+\frac{l}{r}\right), \tag{14}$$

$$\hat{T}_l{}^-=\left(\frac{\partial}{\partial r}+\frac{l}{r}\right)\left(\frac{\partial}{\partial r}+\frac{l+1}{r}\right). \tag{15}$$

The system (12) is obtained bearing in mind that the curl curl operator acting on vectors written down in the form of columns reduces to the operator $(\nabla\hat{\mathbf{I}})$.[2]

Outside the sphere where $r>a$ we have $\mathbf{P}=0$ and the solution of Eq. (6) with the same angular dependence as in the range $r<a$ are sought in the form

$$\mathbf{E}=w^-(r)\mathbf{Y}_{F,\,F-1,\,M}+w^+(r)\mathbf{Y}_{F,\,F+1,\,M}. \tag{16}$$

The functions w^+ and w^- satisfy the equations

$$\begin{aligned}
&\frac{F+1}{2F+1}\Delta_{F-1}w^- +\frac{[F(F+1)]^{1/2}}{2F+1}\hat{T}^-_{F+1}w^+ =-\varkappa_m\frac{\omega^2}{c^2}w^-,\\
&\frac{F}{2F+1}\Delta_{F+1}w^+ +\frac{[F(F+1)]^{1/2}}{2F+1}\hat{T}^+_{F-1}w^- =-\varkappa_m\frac{\omega^2}{c^2}w^+.
\end{aligned} \tag{17}$$

The solutions of the system (12) for the inner part of the sphere are sought in the form

$$\begin{aligned}
&u^-=Aj_{F-1}(qr), \quad v^-=Mj_{F-1}(qr),\\
&u^+=Bj_{F+1}(qr), \quad v^+=\Lambda j_{F+1}(qr),
\end{aligned} \tag{18}$$

where $j_l(qr)$ are spherical Bessel functions related to Bessel functions with a half-integral index by

$$j_l(x)=\left(\frac{\pi}{2x}\right)^{1/2}J_{l+1/2}(x).$$

Substituting the system (18) into the system (12), we obtain the following system of equations for the coefficients A, B, M, and Λ:

$$\begin{aligned}
&-\frac{F+1}{2F+1}q^2M+\frac{[F(F+1)]^{1/2}}{2F+1}q^2\Lambda=-\frac{\omega^2}{c^2}(\varkappa_\infty M+4\pi A),\\
&-\frac{F}{2F+1}q^2\Lambda+\frac{[F(F+1)]^{1/2}}{2F+1}q^2M=-\frac{\omega^2}{c^2}(\varkappa_\infty\Lambda+4\pi M),
\end{aligned}$$

$$A(\hbar^2q^2/2m-\varepsilon)=\alpha M, \quad B(\hbar^2q^2/2m-\varepsilon)=\alpha\Lambda. \tag{19}$$

The condition for solubility of this system reduces to the dispersion equation for optical exciton waves[11]:

$$\left(\varepsilon-\hbar\omega_{LT}-\frac{\hbar^2q^2}{2m}\right)\left[\varkappa_\infty\frac{\omega^2}{c^2}\left(1-\frac{\hbar\omega_{LT}}{\varepsilon-\hbar^2q^2/2m}\right)-q^2\right]=0. \tag{20}$$

It has three solutions. One of these solutions corresponds to a longitudinal exciton

$$\begin{aligned}
&q=\frac{1}{\hbar}\{2m(\varepsilon-\hbar\omega_{LT})\}^{1/2}=q_l, \quad A_l=-\frac{M_l\varkappa_\infty}{4\pi},\\
&B_l=-\left[\frac{F+1}{F}\right]^{1/2}\frac{M_l\varkappa_\infty}{4\pi}, \quad \Lambda_l=\left[\frac{F+1}{F}\right]^{1/2}M_l.
\end{aligned} \tag{21}$$

Two other solutions describe a mixed state of a transverse exciton and an optical wave. The terms with $q\sim 1/a$ are important in the calculation of the size quantization levels. Since the sphere radius is much less than the optical wavelength

$$a\ll c/\omega, \tag{22}$$

we find that $q\gg\omega/c$. For these values of q the exciton and optical branches are weakly coupled so that the solution of the system (19) corresponding to transverse excitons is of the following form in the limit $(m\varepsilon/\hbar)^{1/2}\gg\omega/c$:

$$\begin{aligned}
&q=\frac{1}{\hbar}(2m\varepsilon)^{1/2}=q_t, \quad A_t=\frac{m\varepsilon c^2}{2\pi\hbar^2\omega^2}M_t,\\
&B_t=-\frac{m\varepsilon c^2}{2\pi\hbar^2\omega^2}\left[\frac{F}{F+1}\right]^{1/2}M_t, \quad \Lambda_t=-\left[\frac{F}{F+1}\right]^{1/2}M_t,
\end{aligned} \tag{23}$$

and the solution corresponding to an optical wave is

$$\begin{aligned}
&q=\varkappa_\infty{}^{1/2}\frac{\omega}{c}=q_L, \quad A_L=-\frac{\alpha M_L}{\varepsilon},\\
&B_L=\left[\frac{F}{F+1}\right]^{1/2}\frac{\alpha M_L}{\varepsilon}, \quad \Lambda_L=-\left[\frac{F}{F+1}\right]^{1/2}M_L.
\end{aligned} \tag{24}$$

The electric field outside the sphere is described by

$$\begin{aligned}
&w^-=Hj_{F-1}(kr)+G\mathcal{N}_{F-1}(kr),\\
&w^+=-\left[\frac{F}{F+1}\right]^{1/2}(Hj_{F+1}(kr)+G\mathcal{N}_{F+1}(kr)),
\end{aligned} \tag{25}$$

where $k=\varkappa_m^{1/2}\omega/c$; $\mathcal{N}_F(x)$ are spherical Neumann functions.

It follows from the Pekar boundary condition for the exciton contribution to the polarization that

$$u^-(a)=A_l j_{F-1}(q_l a)+A_t j_{F-1}(q_t a)+A_L j_{F-1}(q_L a)=0, \quad (26)$$

$$u^+(a)=B_l j_{F+1}(q_l a)+B_t j_{F+1}(q_t a)+B_L j_{F+1}(q_L a)=0. \quad (27)$$

It is clear from Eqs. (21), (23), and (24) that the coefficients A_l and B_l, A_t and B_t, A_L and B_L are all of the same order of magnitude. On the other hand, it follows from the condition (22) that $q_L a \ll 1$, so that the third term in Eq. (27) can be ignored. Then, using Eqs. (26) and (27), we can express the amplitudes M_l and M_t of the electric field of longitudinal and transverse waves in terms of the amplitude M_L of the electric field in the optical wave:

$$M_l = -\frac{\hbar\omega_{LT}}{\varepsilon} \times \frac{j_{F-1}(q_L a) j_{F+1}(q_l a)}{j_{F-1}(q_l a) j_{F+1}(q_l a)+(F+1)F^{-1} j_{F-1}(q_l a) j_{F+1}(q_l a)} M_L, \quad (28)$$

$$M_t = \frac{F+1}{F}\left(\frac{\varkappa_\infty \omega^2}{c^2 q_t^2}\right) \times \frac{j_{F-1}(q_L a) j_{F+1}(q_t a)}{j_{F-1}(q_t a) j_{F+1}(q_t a)+(F+1)F^{-1} j_{F-1}(q_t a) j_{F+1}(q_t a)} M_L. \quad (29)$$

It is clear from Eqs. (28) and (29) that $M_t/M_l \sim (a\omega/c)^2 \ll 1$.

We shall now use the conditions that the normal component of the induction and the tangential component of the electric field be continuous at the boundary of a sphere. The normal component of the induction vector is $\mathbf{D}_n = \mathbf{n}(\mathbf{D}\cdot\mathbf{n})$, where $\mathbf{n} = \mathbf{r}/r$ is the vector of the normal to the surface of the sphere. We can show that the operator representing the projection along the normal reduces to the operator $1 - (\hat{\mathbf{l}}\cdot\mathbf{n})^2$ when it is applied to vectors written in the column form [see Eqs. (9) and (10)]. Inside the sphere, we have

$$\mathbf{D}=(\varkappa_\infty v^- + 4\pi u^-)\mathbf{Y}_{F,F-1,M}+(\varkappa_\infty v^+ + 4\pi u^+)\mathbf{Y}_{F,F+1,M}. \quad (30)$$

Outside the sphere the induction vector is $\mathbf{D} = \varkappa_m \mathbf{E}$, where $\mathbf{E}$ is given by Eq. (16). Therefore, the condition of continuity of the normal components of the induction vector at $r = a$ is

$$\varkappa_\infty (v^-(a)F^{1/2} - v^+(a)(F+1)^{1/2}) = \varkappa_m (w^-(a)F^{1/2} - w^+(a)(F+1)^{1/2}). \quad (31)$$

Equation (31) is derived using the Pekar condition of Eqs. (26) and (27), and also the relationship

$$[1-(\hat{\mathbf{l}}\mathbf{n})^2]\mathbf{Y}_{F,F-1,M} = \frac{F}{2F+1}\mathbf{Y}_{F,F-1,M} - \frac{[F(F+1)]^{1/2}}{2F+1}\mathbf{Y}_{F,F+1,M}, \quad (32)$$

$$[1-(\hat{\mathbf{l}}\mathbf{n})^2]\mathbf{Y}_{F,F+1,M} = \frac{F+1}{2F+1}\mathbf{Y}_{F,F+1,M} - \frac{[F(F+1)]^{1/2}}{2F+1}\mathbf{Y}_{F,F-1,M}. \quad (33)$$

The condition of continuity of the tangential component of the electric field vector $\mathbf{E}_\tau = \mathbf{E} - \mathbf{n}(\mathbf{n}\cdot\mathbf{E})$ can similarly be represented in the form

$$v^-(a)(F+1)^{1/2} + v^+(a)F^{1/2} = w^-(a)(F+1)^{1/2} + w^+(a)F^{1/2}. \quad (34)$$

We shall now write down the explicit expressions for $v^+(a)$ and $v^-(a)$:

$$v^+(a) = \left[\frac{F+1}{F}\right]^{1/2} M_l j_{F+1}(q_l a) - \left[\frac{F}{F+1}\right]^{1/2} M_t j_{F+1}(q_t a) - \left[\frac{F}{F+1}\right]^{1/2} M_L j_{F+1}(q_L a), \quad (35)$$

$$v^-(a) = M_l j_{F-1}(q_l a) + M_t j_{F-1}(q_t a) + M_L j_{F-1}(q_L a). \quad (36)$$

Substituting Eqs. (25), (35), and (36) into Eqs. (31) and (34) and bearing in mind that $M_t \ll M_l$, we obtain a system relating the amplitudes M_l and M_L of the electric field of the longitudinal and optical waves inside the sphere with the amplitudes H and G characterizing the electric field outside the sphere:

$$\frac{\varkappa_\infty}{F^{1/2}} M_l [F j_{F-1}(q_l a) - (F+1) j_{F+1}(q_l a)] + \varkappa_\infty F^{1/2} M_L j_{F-1}(q_L a) = \varkappa_m F^{1/2} [H j_{F-1}(ka) + G\mathcal{N}_{F+1}(ka)], \quad (37)$$

$$(F+1)^{1/2} M_l (j_{F-1}(q_l a) + j_{F+1}(q_l a)) + (F+1)^{1/2} M_L j_{F-1}(q_L a) = (F+1)^{1/2} H j_{F-1}(ka) - F(F+1)^{-1/2} G\mathcal{N}_{F+1}(ka). \quad (38)$$

The asymptotic behavior of the electric field in the limit $r \to \infty$ is given by

$$E \sim [\sin(kr - \pi F/2 + \delta_F)]/r.$$

It is clear from Eq. (25) that the scattering phase δ_F is related to the coefficients H and G by

$$\operatorname{tg}\delta_F = G/H. \quad (39)$$

The final expression for the scattering phase is obtained by determining the ratio G/H from Eqs. (37) and (38) and application of the relationship (28) between the coefficients M_l and M_L:

$$\operatorname{tg}\delta_F = \frac{\pi(F+1)}{F(F+1/2)\Gamma^2(F+1/2)} \times \left(\frac{ka}{2}\right)^{2F+1} \frac{(\varkappa-1)\Phi(\varepsilon) - (\varkappa + F/(F+1))}{(\varkappa + (F+1)/F)\Phi(\varepsilon) - (\varkappa-1)}, \quad (40)$$

where $F = 1,2,3,...$; $\Gamma(x)$ is the gamma function; $\varkappa = \varkappa_\infty/\varkappa_m$ is a function described by

$$\Phi(\varepsilon) = \frac{F}{F+1}\left(1 - \frac{\varepsilon}{\hbar\omega_{LT}}\right)\frac{j_{F-1}(q_l a)}{j_{F+1}(q_l a)} - \frac{\varepsilon}{\hbar\omega_{LT}}\frac{j_{F-1}(q_t a)}{j_{F+1}(q_t a)}. \quad (41)$$

In the derivation of Eq. (40) we used the smallness of the parameter ka, replacing the functions $j_{F-1}(ka)$ and $\mathcal{N}_{F+1}(ka)$ with their asymptotic forms.

It is clear from Eq. (40) that the scattering phase is small, $\tan\delta_F \sim \delta_F \sim (ka)^{2F+1} \ll 1$, because the sphere is small compared with the optical wavelength on the basis of the condition (22). An exception to this rule is the case when the denominator of Eq. (40) vanishes, i.e., when

$$\Phi(\varepsilon)=\frac{\varkappa-1}{\varkappa+(F+1)/F}. \tag{42}$$

As pointed out above [see Eq. (8)] this occurs at optical frequencies corresponding to the creation of an exciton at a size quantization level. For each value of F there is an infinite series of such levels $\varepsilon_F^{(n)}$, the positions of which are determined by the condition (42). We can find the radiative width of a level $\Gamma_F^{(n)}$ by expanding the denominator in Eq. (40) near the value $\varepsilon=\varepsilon_F^{(n)}$ and representing the expression for the phase δ_F in the form of Eq. (8). We then obtain

$$\Gamma_F^{(n)}=\frac{2\pi}{F^2}\frac{2F+1}{\Gamma^2(F+1/2)} \times\frac{\varkappa}{(\varkappa+(F+1)/F)^2}\frac{1}{|\Phi'(\varepsilon_F^{(n)})|}\left(\frac{ka}{2}\right)^{2F+1}. \tag{43}$$

We can see that the maximum width, i.e., the minimum radiative lifetime, is exhibited by the states with $F=1$.

In addition to the size quantization levels at positions given by Eq. (42), there are also levels which are characterized by a different angular dependence of the electric field $\mathbf{E}$ and of the polarization $\mathbf{P}$, proportional to $\mathbf{Y}_{F,F,M}$ as given by Eqs. (9) and (10). For a given value of F these states differ in parity from those discussed above. The positions of the corresponding levels and their radiative widths can be found from the scattering phases, the expressions of which can be obtained by the same method as in Eq. (40). We give only the final answer:

$$\operatorname{tg}\delta_F=-\frac{2\pi(F+1)}{(F+1/2)^2\Gamma^2(F+1/2)} \times\left(\frac{\varkappa\hbar\omega_{LT}}{\varepsilon}\right)\left(\frac{1}{q_t a}\frac{j_{F+1}(q_t a)}{j_F(q_t a)}\right)\left(\frac{ka}{2}\right)^{2F+3}. \tag{44}$$

We can see that the level positions are governed by the condition $j_F[(2m\varepsilon_F^{(n)})^{1/2}a/\hbar]=0$, i.e., the situation is exactly the same as in the absence of the longitudinal-transverse splitting ($\omega_{LT}\to 0$).[8] The minimum lifetime corresponds to the levels with $F=1$ and—in order of magnitude—it is $(ka)^2$ times longer than for the levels of different parity, but also with $F=1$ [see Eqs. (40) and (43)].

In addition to the states described above, there are also states with $F=0$. In the case of these states the angular dependences of $\mathbf{E}$ and $\mathbf{P}$ are proportional to $\mathbf{Y}_{010}$ and are purely longitudinal ($\operatorname{curl}\mathbf{E}=\operatorname{curl}\mathbf{P}=0$). For these states the electric field differs from zero only inside the investigated sphere, so that their radiative width is zero. The positions of the levels are governed by the condition

$$j_1((2m(\varepsilon^{(n)}-\hbar\omega_{LT}))^{1/2}a/\hbar)=0.$$

4. POSITIONS AND LIFETIMES OF OPTICALLY ACTIVE LEVELS

It follows from the above analysis that of all the states we have found the shortest radiative lifetime (in terms of the parameter ka) is exhibited by the levels with $F=1$, which we shall call optically active. The positions of these levels are described by the equation

$$\left[\frac{1}{2}\frac{j_0(q_t a)}{j_2(q_t a)}+\frac{j_0(q_t a)}{j_2(q_t a)}\right]\left[\varkappa\left(1-\frac{\hbar\omega_{LT}}{\varepsilon}\right)+2\right] =\frac{\hbar\omega_{LT}}{\varepsilon}\left\{\frac{j_0(q_t a)}{j_2(q_t a)}+1-\varkappa\left[\frac{j_0(q_t a)}{j_2(q_t a)}+1\right]\right\}, \tag{45}$$

which is obtained from Eq. (42) by substituting $F=1$. We solve this equation numerically for $\varkappa_\infty=3.7$, $\varkappa_m=2.25$, and $\varkappa=1.65$ which corresponds to spheres of CuCl in an insulating silicate glass matrix.[13] Figure 2a shows the dependences of the position of the four lowest levels on the dimensionless parameter $\theta=\hbar/2ma^2\omega_{LT}$ found by solving the above equation. We can see that at low values of θ the dependence $\varepsilon(\theta)$ is linear. This can be demonstrated analytically as follows. Since $\varepsilon\ll\hbar\omega_{LT}$ if $\theta\ll 1$, it follows that we need retain only those terms in Eq. (45) which contain the large parameter $\hbar\omega_{LT}/\varepsilon$. This equation then reduces to $j_2(q_t a)=0$. Hence, we obtain $\varepsilon_n=\hbar^2\varphi_n^2/2ma^2$, where φ_n are the roots of a spherical Bessel function $j_2(x)$. Including the first correction in respect of the small parameter θ, we now find that the level positions are given by

$$\varepsilon_n=\hbar\omega_{LT}\theta\varphi_n^2\left[1-\frac{4(\varkappa+2)}{3\varkappa}\varphi_n\frac{j_0(\varphi_n)}{j_2'(\varphi_n)}\theta\right]. \tag{46}$$

At high values of θ the dependence $\varepsilon(\theta)$ is also linear (Fig. 2a). We can describe it analytically bearing in mind that since the inequality $\varepsilon\gg\hbar\omega_{LT}$ is obeyed in this range, then in the zeroth approximation we can ignore the longitudinal-transverse splitting in the determination of the level positions. Assuming that $\omega_{LT}=0$, we find from Eq. (45) that

$$j_0(q_l a)j_2(q_t a)=-2j_0(q_t a)j_2(q_t a).$$

In the limit $\omega_{LT}\to 0$, we have $q_l=q_t$, so that there are two systems of levels

$$\varepsilon_{2n-1}=\hbar^2\pi^2n^2/2ma^2,\quad \varepsilon_{2n}=\hbar^2\varphi_n^2/2ma^2.$$

For finite values of ω_{LT} and $\theta\gg 1$, the expressions for ε_n become

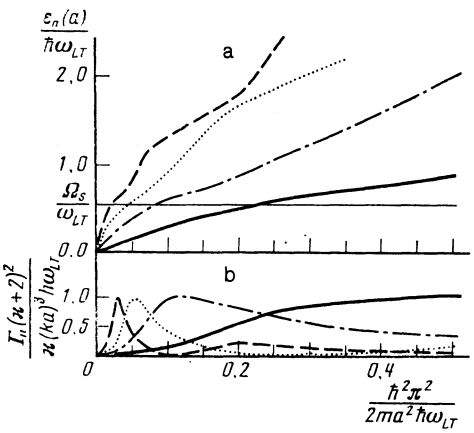

FIG. 2. Dependence of the positions of the four lowest size-quantization levels ε_n (a) and of the reciprocal of the radiative lifetime Γ_n of these levels [in units of $(ka)^3\varkappa\hbar\omega_{LT}/(\varkappa+2)^2$] (b) on the radius of a semiconductor sphere. These calculations were carried out for $\varkappa=\varkappa_\infty/\varkappa_m=1.65$.

$$\varepsilon_{2n-1}=\frac{\hbar^2\pi^2n^2}{2ma^2}+\hbar\omega_{LT}\left[\frac{1}{3}+\frac{4(\varkappa-1)}{(\varkappa+2)\pi^2n^2}\right], \quad (47)$$

$$\varepsilon_{2n}=\frac{\hbar^2\varphi_n^2}{2ma^2}+\frac{2}{3}\hbar\omega_{LT}. \quad (48)$$

It is also clear from Fig. 2a that the dependences $\varepsilon_n(\theta)$ for all the size quantization levels n have a point of inflection at values of θ for which $\varepsilon_n(\theta)$ is close to $\hbar\Omega_s=\hbar(\omega_s^{(1)}-\omega_T)=\hbar\omega_{LT}/(1+2/\varkappa)$ [see Eq. (3)], where $\omega_s^{(1)}$ is the frequency of a surface mode for states with the total momentum $F=1$. We shall henceforce refer to the quantity $\hbar\Omega_s$ as the energy of a surface exciton. It is possible to study analytically the behavior of the dependences $\varepsilon_n(\theta)$ in the range $|\varepsilon_n(\theta)-\hbar\Omega_s|\ll\hbar\omega_{LT}$ only in the case of levels with high numbers $n\gg1$. We shall do this by rewriting Eq. (45) in the form

$$\frac{\varepsilon}{\hbar\Omega_s}-1=\left[\frac{1}{q_la}\frac{j_1(q_la)}{j_2(q_la)}-\frac{\varkappa}{q_la}\frac{j_1(q_la)}{j_2(q_la)}\right]\varkappa^{-1}\times\left[-\frac{1}{2}+\frac{1}{q_la}\frac{j_1(q_la)}{j_2(q_la)}+\frac{1}{2q_la}\frac{j_1(q_la)}{j_2(q_la)}\right]^{-1}. \quad (49)$$

We shall show later that the values of $\theta=\theta_n$ characterized by $\varepsilon_n(\theta)=\hbar\Omega$ are small when n is large ($\theta_n\ll1$ when $n\gg1$). On the other hand, if $\varepsilon=\hbar\Omega_s$, then $q_la=1/(1+2/\varkappa)\theta^{1/2}$ and $q_la=i|q_la|=2i/(\varkappa+2)\theta^{1/2}$, so that $q_la\gg1$ and $|q_la|\gg1$, which allows us to replace the spherical Bessel functions in Eq. (49) with their asymptotic expressions. This gives

$$\frac{\varepsilon}{\hbar\Omega_s}-1=2\left(\theta\frac{\varkappa+2}{\varkappa}\right)^{1/2}\left[\operatorname{ctg}\left(\frac{\varepsilon}{\hbar\Omega_s}\frac{\varkappa}{(\varkappa+2)\theta}\right)^{1/2}+\left(\frac{1}{2\varkappa}\right)^{1/2}\right]. \quad (50)$$

Equation (50) readily yields the values

$$\theta_n=\varkappa/(\varkappa+2)\,(\pi n-\operatorname{arctg}(2\varkappa)^{1/2})^2.$$

We now expand the right-hand side of this equation near $\varepsilon=\hbar\Omega_s$. Introducing the notation $y=(\varepsilon/\hbar\Omega_s-1)[\varkappa/4\theta(\varkappa+2)]^{1/2}$, we can reduce Eq. (50) to

$$y=\operatorname{ctg}\left(\left[\frac{\varkappa}{\theta(\varkappa+2)}\right]^{1/2}+y\right)+\frac{1}{(2\varkappa)^{1/2}}. \quad (51)$$

We can now readily show that the dependence $y(\theta)$ implicitly defined by Eq. (51) has a point of inflection at values

$$\theta=\tilde\theta_n=\varkappa/(\varkappa+2)\,(\pi n-\pi/2-(2\varkappa)^{-1/2})^2,$$

where the cotangent vanishes. We then have $y=(2\varkappa)^{-1/2}$ and the positions of the levels at the point of inflection are described by

$$\varepsilon_n(\tilde\theta_n)=\hbar\Omega_s\left(1+\sqrt{\frac{2}{\varkappa}}\frac{1}{\pi n}\right).$$

We have thus shown that in the case of levels with high numbers a point of inflection appears in the dependence $\varepsilon_n(\theta)$ when the energy is close to that of a surface exciton. It is clear from Fig. 2a that this does indeed occur for all the size-quantization levels, beginning from the ground state.

It must be pointed out that the presence of an inflection point in the dependence $\varepsilon_n(\theta)$ gives rise to a sharp maximum in the dependence $\Gamma_n(\theta)$ describing the radiative width of a size-quantization level [see Eq. (43)]. In other words, the shortest radiative lifetime is exhibited by exciton states in spheres when the size quantization levels are close to the energy of a surface exciton.[1)] This can be illustrated by considering the example of levels with high serial numbers. Simplifying Eq. (43) with $F=1$ in the same way as in the derivation of Eq. (49), we obtain

$$\Gamma_n(\theta)=\frac{\Gamma_n(\tilde\theta_n)\sin^2\left(\left[\frac{\varkappa}{\theta(\varkappa+2)}\right]^{1/2}+y\right)}{1+\sin^2\left(\left[\frac{\varkappa}{\theta(\varkappa+2)}\right]^{1/2}+y\right)}$$

$$=\frac{\Gamma_n(\tilde\theta_n)}{(y-(2\varkappa)^{-1/2})^2+2}, \quad (52)$$

where

$$\Gamma_n(\tilde\theta_n)=2(ka)^3\varkappa\hbar\omega_{LT}/(\varkappa+2)^2 \quad (53)$$

is the width of a level at the inflection point $\theta=\tilde\theta_n$ and the dependence $y(\theta)$ is described by Eq. (51). The second equation in Eq. (52) is obtained from Eq. (51). It follows from Eq. (52) that the level width differs considerably from zero in a region $|y-(2\varkappa)^{-1/2}|\sim1$, which corresponds to the following interval of the parameter θ: $|\theta-\theta_n|\sim1/(\pi n)^2$; the corresponding energy interval is $|\varepsilon-\hbar\Omega_s|\sim\hbar\Omega_s/\pi n$. The calculated dependences of the level width on the parameter θ are plotted in Fig. 2b for the four lowest levels. We can see that the maxima appear in these dependences at $\varepsilon\approx\hbar\Omega_s$ for all the levels, with the exception of the ground state. These maxima become narrower on increase in the serial number of the level and the value of the level with the maximum is described well by Eq. (53).

5. COMPARISON WITH THE EXPERIMENTAL RESULTS

The theory developed in the preceding section allows us to calculate the form of the exciton luminescence spectrum:

$$I(\hbar\omega)\sim\sum_n\int_0^\infty da\,p(a)\Gamma_n(a)\delta(\hbar\omega-\varepsilon_n(a)-\hbar\omega_T), \quad (54)$$

where $\Gamma_n(a)$ and $\varepsilon_n(a)$ are the radiative width and the position of the nth size quantization level in a sphere of radius a; $p(a)$ is the function describing the size distribution of the spheres. Equation (54) is derived on the assumption that the populations of all the size quantization levels are the same. Calculation of the integral in Eq. (54) yields

$$I(\hbar\omega)\sim\sum_n p(a_{n,\omega})\Gamma_n(a_{n,\omega})\left|\frac{\partial\varepsilon_n}{\partial a}\right|^{-1}, \quad (55)$$

where $a_{n,\omega}$ is the value of the radius at which the argument of the δ function vanishes. The derivative $\partial\varepsilon_n/\partial a$ can be found by varying Eq. (42) so as to determine the size quantization levels.

The size distribution of the spheres was considered in

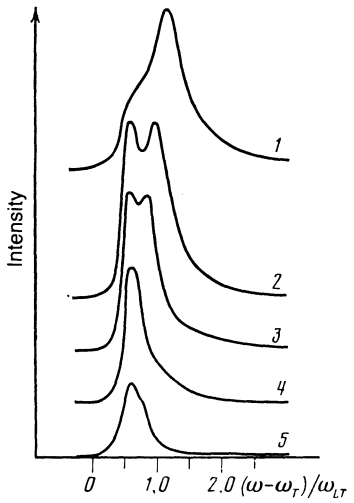

FIG. 3. Theoretical luminescence spectra calculated for different average radii of microcrystals using Eq. (56): 1) $\bar{a}=56$ Å; 2) $\bar{a}=62$ Å; 3) $\bar{a}=70$ Å; 4) $\bar{a}=95$ Å; 5) $\bar{a}=132$ Å.

Ref. 4. It was found experimentally that it is described satisfactorily by the Lifshitz-Slezov distribution[15] obtained by an analysis of the supercondensation stage of precipitation of a phase from a supersaturated solid solution:

$$p_0(x)=\begin{cases}\dfrac{3^4ex^2\exp[-1/(1-2x/3)]}{(x+3)^{7/3}(1.5-x)^{11/3}}, & x<1.5\\ 0, & x>1.5\end{cases}, \qquad (56)$$

where $x=a/\bar{a}$; $\bar{a}$ is the average radius of the spheres dependent on the supercondensation time $t(\bar{a}\propto t^{1/2})$, as shown in Ref. 15. Equation (56) is an asymptotic expression in the limit of long times ($\ln t\gg 1$). It is shown in Refs. 16 and 17 that for finite times the distribution function does not terminate at $a>1.5\bar{a}$ and numerous mechanisms for the termination of the "tails" of the distribution function in the range of large sizes have been considered. Therefore, in numerical calculations based on Eq. (55) we assumed the following model distribution function:

$$p(x)=\begin{cases}p_0(x), & x<x_c=1.23\\ \alpha/x^{4.2}+\beta/x^8, & x>x_c\end{cases}. \qquad (57)$$

The coefficients α and β were selected from the conditions that the function $p(x)$ and its derivative be continuous at the point x_c. The results of a numerical calculation of the luminescence spectra are given in Fig. 3 for various values of the average radius of the spheres. We can see that the calculated curves reproduce qualitatively the main features of the experimental spectra: the appearance (beginning from a certain average size) of a second maximum and the rise of its intensity at the same position as the average size increases. We shall now account for this result qualitatively.

It is shown in Sec. 4 that the radiative lifetime of excitons at all the excited levels, beginning from the first, has a sharp minimum where the position of the size quantization level $\varepsilon_n(a)$ coincides with the energy of a surface exciton $\hbar\Omega_s$. In other words, the excited states contribute to the luminescence only in microcrystals which satisfy $|\varepsilon-\Omega_s|\ll\hbar\Omega_s$. At low values of the average radius ($\bar{a}\sim 50$ Å) the ground-state energy is of the order of $\hbar^2\pi^2/2ma^2\approx 15$ meV for all the microcrystals, i.e., it is considerably greater than $\hbar\Omega_s=2.5$ meV, so that in this case there are no microcrystals with the levels close to $\hbar\Omega_s$ and the spectrum exhibits one line representing the luminescence of excitons at the lowest size-quantization level (curve 1 in Fig. 1). As the average size $\bar{a}$ increases, microcrystals satisfy this condition and the second line appears at the frequency $\Omega_s+\omega_T$ (curve 2). A further increase in the average size of microcrystals does not affect the position of the new line, but its intensity continues to rise (curves 3 and 4) because of an increase in the number of microcrystals in which the position of excited size-quantization levels is close to $\hbar\Omega_s$. On the other hand, we can see from Fig. 2b that the radiative lifetime at the ground state begins to rise considerably on increase in the microcrystal size when the energy of this state becomes less than $\hbar\Omega_s$. Therefore, in the range of large sizes the ground size-quantization state makes no contribution to the luminescence.

The authors are deeply grateful to M. I. D'yakonov, E. L. Ivchenko, V. A. Kiselev, V. I. Sugakov, and I. A. Éfros for valuable discussions, and to V. V. Slezov for supplying a detailed bibliography on the critical coalescence in solid solutions.

[1)]This was also pointed out in Ref. 14. In that investigation a numerical calculation was made of the absorption coefficient of an insulating sphere allowing for spatial dispersion. The spectral dependence of the absorption coefficient was found to have a maximum when the frequency of the incident light coincides with ω_s.

[1]V. V. Golubkov, A. I. Ekimov, A. A. Onushchenko, and V. A. Tsekhomskiĭ, Fiz. Khim. Stekla **7**, 397 (1981).
[2]A. I. Ekimov and A. A. Onushchenko, Pis'ma Zh. Eksp. Teor. Fiz. **40**, 337 (1984) [JETP Lett. **40**, 1136 (1984)].
[3]A. I. Ekimov and A. A. Onushchenko, Pis'ma Zh. Eksp. Teor. Fiz. **34**, 363 (1981) [JETP Lett. **34**, 345 (1981)].
[4]A. I. Ekimov, A. A. Onushchenko, A. G. Plyukhin, and Al. L. Éfros, Zh. Eksp. Teor. Fiz. **88**, 1490 (1985) [Sov. Phys. JETP **61**, 891 (1985)].
[5]T. Mita, K. Sotome, and M. Ueta, J. Phys. Soc. Jpn. **48**, 496 (1980).
[6]S. I. Pekar, Zh. Eksp. Teor. Fiz. **33**, 1022 (1957) [Sov. Phys. JETP **6**, 785 (1958)].
[7]Yu. I. Petrov, Fizika malykh chastits (Physics of Small Particles), Nauka, M., 1982, p. 359.
[8]J. J. Hopfield and D. G. Thomas, Phys. Rev. **132**, 563 (1963).
[9]J. D. Jackson, Classical Electrodynamics, Wiley, New York, 1962 (Russ. Transl., Mir, M., 1965).
[10]A. I. Akhiezer and V. B. Berestetskiĭ, Kvantovaya élektro-dinamika, Nauka, M., 1969 (Quantum Electrodynamics, Interscience, New York, 1965).
[11]M. Born and K. Huang, Dynamical Theory of Crystal Lattices, Oxford University Press, 1954 (Russ. Transl., IL, M., 1958).
[12]Al. L. Éfros and A. L. Éfros, Fiz. Tekh. Poluprovodn. **16**, 1209 (1982) [Sov. Phys. Semicond. **16**, 772 (1982)].
[13]Y. Kaifu and T. Komatsu, J. Phys. Soc. Jpn. **25**, 644 (1968).
[14]I. Yu. Golineĭ and V. I. Sugakov, Fiz. Nizk. Temp. **11**, 775 (1985) [Sov. J. Low Temp. Phys. **11**, 427 (1985)].
[15]I. M. Lifshitz and V. V. Slezov, Zh. Eksp. Teor. Fiz. **35**, 479 (1958) [Sov. Phys. JETP **8**, 331 (1959)].
[16]I. M. Lifshitz and V. V. Slezov, Fiz. Tverd. Tela (Leningrad) **1**, 1401 (1959) [Sov. Phys. Solid State **1**, 1285 (1960)].
[17]V. V. Slezov and V. V. Sagalovich, J. Phys. Chem. Solids **38**, 943 (1977).

Translated by A. Tybulewicz